ACS APPLIED MATERIALS & INTERFACES

RESEARCH ARTICLE

www.acsami.org

Fundamental Examination of Nanoparticle Heating Kinetics Upon Near Infrared (NIR) Irradiation

Amanda M. Schrand,[†] Bradley M. Stacy,[†] Sarah Payne,[‡] Larry Dosser,[‡] and Saber M. Hussain*[,†]

[†]Applied Biotechnology Branch, Human Effectiveness and Protection Directorate, 711th Human Performance Wing, Wright-Patterson Air Force Base, Ohio 45433-5707, United States

[‡]Mound Laser & Photonics Center (MLPC), Inc., PO Box 223, Miamisburg, Ohio 45343-0223, United States

ABSTRACT: Near infrared (NIR) light, which spans wavelengths from ~700−1100 nm holds particular promise in bionanotechnology-enabled applications because both NIR light and nanoparticles (NPs) have the potential for remote activation leading to exquisite localization and targeting scenarios. In this study, aqueous solutions of carbon and metal-based NPs (carbon black, single-walled carbon nanotubes, silver nanoparticles and copper nanoparticles) were exposed to continuous NIR laser (λ = 1064 nm) irradiation at powers of 2.2W and 4.5W. The differential heating of bulk aqueous suspension of NPs with varying physicochemical properties revealed maximum temperatures of 67 °C with visible evidence of condensation and bubble formation. The basis of the NP heating is due to the strong intrinsic optical absorbance in the NIR spectral window and the transduction of this NIR photon energy into thermal energy. In this regard, UV−vis measurements can accurately predict NP heating kinetics prior to NIR irradiation. Further, a uniform thermodynamic heating model demonstrates close agreement with the experimental data for the low NIR-absorbing NPs. However, the uniform thermodynamic heating model used in this study does not accurately portray the energy release upon localized NP heating because of bubble formation for the highly absorbing NPs. Therefore, this study reveals the differential heating kinetics of NPs excited with NIR with implications in the development of novel NIR-NP-based systems.

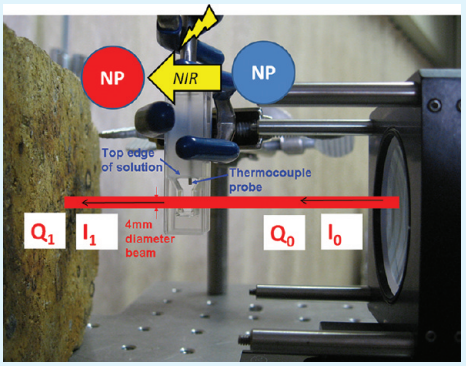

KEYWORDS: near-infrared laser, NIR, nanoparticles, temperature kinetics, spectroscopy, exothermic, bionanotechnology, thermodynamic modeling

1. INTRODUCTION

Near infrared (NIR) light, which spans wavelengths from ~700−1100 nm, holds particular promise in bionanotechnology-enabled applications because neither biological molecules nor water absorb light in the NIR frequency range, thus enabling NIR light to pass through tissues or cells to specifically target absorbed nanoparticles (NPs). Several recent studies have shown that increasing concentrations of NPs (i.e., carbon nanotubes, carbon nanohorns, gold nanoparticles), and/or increasing amounts of laser power density delivered to NPs, leads to increased absorbance in the NIR spectral region and subsequent rapid temperature elevations for the NPs and surrounding bulk solutions; for recent reviews, see refs 1−6. In particular, single gold nanoparticles have been examined for direct heating upon NIR exposure.[6−9] Bendix et al.[7] developed a direct method to measure the electromagnetic heating of gold nanoparticles (GNPs) by using supported lipid bilayers. This study showed that it was possible to get the heating profile of a single GNP by quantifying the melting the lipid bilayer. However, for NPs of different shapes, sizes and aggregation state, the surface area may not be accurately measured. Therefore, alternative approaches such as measuring the bulk heating of NP solutions may provide a simpler approach to study the heating kinetics for other nanoparticle compositions that are readily being incorporated into technological innovations.

Although ultrashort laser pulse heating of gold nanoparticles was previously modeled with one- and two-temperature models,[10,11] information is lacking regarding the differential heating kinetics for NPs of varying elemental compositions under identical NIR laser conditions. First assessing the differential heating kinetics of NPs in a standardized acellular environment is important prior to incorporation into biological systems because of the strong implications of NP-induced toxicity. Therefore, in order to determine the role of composition on differential NIR-based heating kinetics, we examined both metal (Ag and Cu) and carbon-based NPs (SWNT, SWNT-COOH, CB), which were previously examined for toxicity in mammalian cell culture[12,13] and have high relevance to both therapeutic and antimicrobial applications.

Further, the choice of NP concentration will determine the efficacy of the treatment at the biological interface. In order to avoid overt toxicity, relatively low doses were initially considered. Examination of the literature returned values for maximum dosages of 300 μg/mL for carbon nanohorns[2] and 25 μg/mL, 1000 μg/mL or even 2000 μg/mL for carbon nanotubes.[1,5,14] However, a saturation plateau was reached at 1000 μg/mL for the

Received: June 30, 2011
Accepted: September 2, 2011
Published: September 02, 2011

SWNTs and at even lower concentrations (~100 μg/mL) for the MWNTs.[5] Further, the laser absorbance plateaus at very high concentrations and it is not necessary to completely saturate the solutions with NPs in order to reach the desired heating effects. Therefore, in this study, we chose a concentration of 50 μg/mL to avoid overt toxicity and maximize laser absorbance while maintaining a high degree of visible dispersion over the duration of the laser exposure.

The application of NIR light at the 1064 nm wavelength, in particular, has demonstrated utility in studies with gold nanoparticles, carbon nanohorns and multiwalled carbon nanotubes, respectively, for biomedical (ie. cancer cell destruction) and antimicrobial/decontamination purposes.[1,3−5,14−16] Laser powers ranging from 1 to 5W for up to 10 min produced maximum NP solution temperatures of 85 °C, which were the highest for concentrations >100 μg/mL; mostly for carbon-based NPs.[1,2,5] Therefore, in this study we chose laser conditions of: λ = 1064 nm at 2.2−4.5 W for up to 5 min.

More complex surface biofunctionalized NPs can act as "capture elements" for highly localized and remote modulation of the bound biomolecules upon NIR laser exposure. For example, the exposure of carbon nanohorns to short times (10−20 s) and powers (1−5W) of 1064 nm laser radiation effectively eradicated bound bacteria such as *S. cerevisiae* or *E. coli*.[2] The observed antimicrobial activity was hypothesized to result from the intense and localized heating occurring that occurred at the interface of the NPs and bacteria.[2] Other work with polyhydroxyalkanoate (PHA) synthase functionalized Au NPs showed promise as a targeted drug delivery agent, in protein purification systems and immunodetection.[17] Further, optics systems can greatly benefit from the addition of nanoparticles that change color or fluorescence with temperature such as Au nanorods[18] or biofunctionalized boron nitride nanotubes.[19]

Therefore, controlling the temperature of such solutions facilitates a wide range of potential applications in sensing, remediation, photodynamic cancer therapy, laser tissue welding, and microsurgery.[20−26]

2. MATERIALS AND METHODS

2.1. Nanoparticles. Nanosized carbon black (CB, Cabot), silver nanoparticles (Ag NPs, Novacentrix), single-walled carbon nanotubes (SWNT, Cheaptubes, Inc.), oxidized single-walled carbon nanotubes (SWNT-COOH, Cheaptubes, Inc.) and copper nanoparticles (Cu NPs, Novacentrix) were weighed and suspended in sterile ddH2O at concentrations of 50 μg/mL in sterile. Characterization of NP size and morphology was performed with transmission electron microscopy (TEM, Philips/FEI Lab6, 200 kV), spectral properties including absorption maxima were examined with UV−vis-NIR spectroscopy, quality of dispersion or average NP agglomerate sizes in solution was examined with dynamic light scattering (DLS, Malvern ZetaSizer) in addition to determination of surface charge through zeta potential measurements (Malvern ZetaSizer) as previously described.[27]

2.2. NIR Laser. A 500 W continuous 1064 nm wave laser was used as the source of NIR. The laser beam was set to deliver either 2.2 W (0.175 W/mm^2, 17.5 W/cm^2 power density) or 4.5 W (0.358 W/mm^2, 35.8 W/cm^2 power density) to the CB, Ag, SWNT, SWNT-COOH, and Cu NP solutions placed into a quartz cuvette. Upon turning the laser beam on, the initial temperature was recorded, then the subsequent temperature recorded every 30 s for 4−5 min (Dostmann Model P650-MP digital thermometer with microprobe sensor), after which the laser was turned off. An empty cuvette was used as a blank control and a cuvette filled with H2O was used as a solution control. Digital images were taken of the solutions in the cuvettes before and after the laser irradiation.

Table 1. Thermodynamic Properties of Solutions

volume (mL)	1
density (g/cm^3)	1
m (grams)	1
p-2.2 W (w/mm^2)	0.18
p-4.5 W (w/mm^2)	0.36
area (mm^2)	12.57
C_v H_2O (J/(g K))	4.14

2.3. Thermodynamic Analysis. The heating kinetics of the NPs were modeled using a combination of the differential form of the first law of thermodynamics and a form of the Beer−Lambert law. When simplifying the first law, phase change is not taken into account due to the inability to measure it at this time point. It is assumed that a negligible amount of water will boil in this closed system. The parameters used are shown in Table 1.

The physical and thermodynamic properties of water were considered unchanged upon the addition of 50 μg/mL of NPs. Based on this hypothesis, the NPs are assumed to contribute negligible effects on the properties at a total liquid weight of only 0.005%. Therefore, the first law of thermodynamics reduces to the following eq 1

$$mC_v dT/dt = Q_{in} - Q_{out} \quad (1)$$

Differentiating the equation leads to eq 2

$$(T_2 - T_1) = [(Q_{in} - Q_{out})\Delta t]/mC_v \quad (2)$$

Q_{out} is the energy being released into the environment from the cuvette due to thermal conduction. This was modeled using data collected when the laser was shut off. The heat flux was modeled as a function of the temperature of the solution. Q_{in} is the energy being absorbed by the system from the laser. This was modeled using Beer−Lamberts law

$$TR = I_1/I_o = 10^{-a} \quad (3)$$

$$Q_{in} = (1 - 10^{-a})PA \quad (4)$$

3. RESULTS

3.1. Nanoparticle Characterization. Nanoparticles (NPs) with different elemental compositions (Ag, C, Cu) were suspended in water at 50 μg/mL, leading to distinct colors and dispersion qualities (Figure 1). The carbon black (CB), silver (Ag), single-walled carbon nanotubes (SWNT) and carboxylic acid-functionalized SWNT (SWNT-COOH) solutions were gray and the copper (Cu) NPs had a yellow hue. The NPs were characterized for size and morphology with bright-field transmission electron microscopy (BF-TEM, Figure 1A2−G2). The nanosized CB and Ag NPs were primarily spherical with average sizes of 20 nm and 25 nm, respectively. The SWNTs were present in bundles both before (Figure 1C2) and after oxidation (SWNT-COOH, Figure 1D2). Copper nanoparticles (Cu NPs) of different sizes (40, 60, and 80 nm) showed rough surface features consistent with oxidation (Figure 1E2−G2).

Bulk solution properties were characterized with dynamic light scattering (DLS) and UV−vis spectroscopy. It is worth mentioning here that no methods were employed to prevent gravitational settling of the NP solutions (ie. additives such as surfactants and/or surface modifications or mechanical agitation such as sonication) during the experiments. Therefore, all of the NPs examined in this study formed agglomerates under these natural

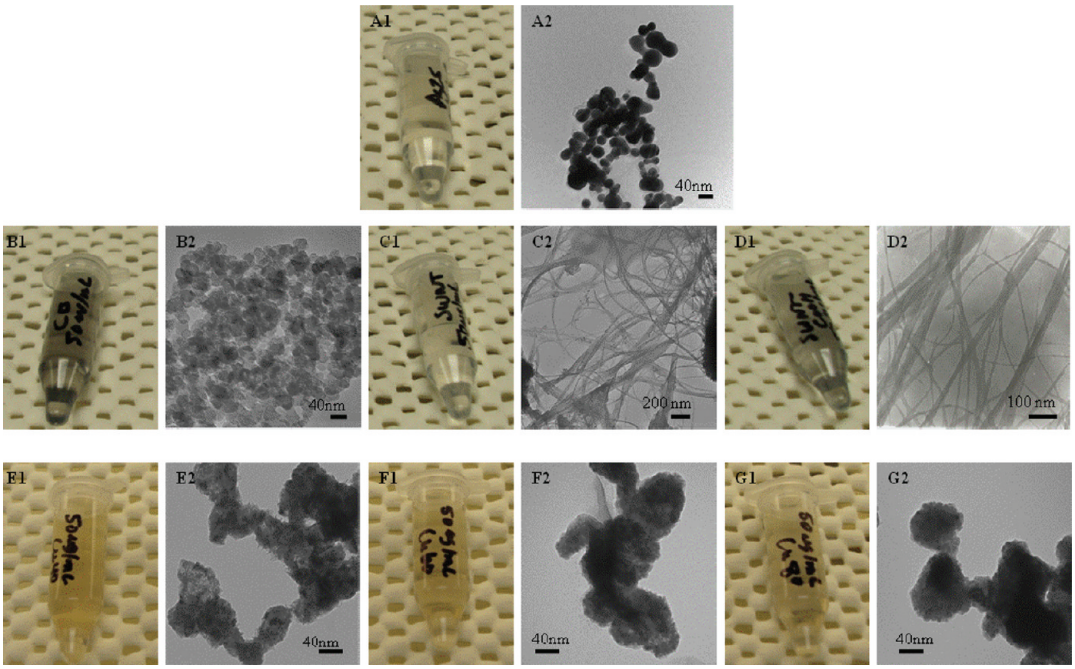

Figure 1. (A1−G1) Digital images and (A2−G2) bright-field transmission electron micrographs (BF-TEM) of nanoparticles. (A) 25 nm Ag NPs, (B) 20 nm Carbon Black NPs, (C) SWNTs, (D) SWNT-COOH, (E) 40 nm Cu NPs, (F) 60 nm Cu NPs, (G) 80 nm Cu NPs.

conditions with much larger sizes in solution compared to their primary sizes (Table 2). To retain the maximum number of NPs within the laser beam pathway and minimize segregation from solution, short laser exposure periods (i.e., 5 min) were chosen.

The toxicity of the various types of NPs were previously examined in neuroblastoma cells at 50 μg/mL over 24 h.[12,13] The Cu NPs demonstrated the greatest toxicity in a size-dependent manner (unpublished data). By comparison, the SWNTs and Ag NPs reduced cell viability by ∼50%. The CB NPs displayed the least toxicity and reduced viability by only 15%.

To understand the relationship between the spectral absorbance of the NP solutions in the NIR range (∼700−1100 nm) and the heat kinetics of the NP solutions after exposure to a laser wavelength of 1064 nm, the NP solutions were first examined with UV−vis−NIR spectroscopy over the entire range of 200−1300 nm (Figure 2, Table 2). Each NP solution had a distinct absorbance profile based on its elemental composition as well as rather smooth spectra or the presence of well-defined peaks. The well-defined peaks in the absorbance spectra can indicate both spectral absorption and a lack of NP aggregation in solution.[1]

In particular, the Ag NPs had very prominent absorbance maxima at ∼414 nm, compared to a small amount of absorbance at >1100 nm (Figure 2A). Although the lower values are outside of the NIR spectral range, they contribute to other useful spectral properties such as plasmon resonance for imaging purposes.[13,28] Maxima for the carbon-based nanomaterials (SWNTs, SWNT-COOH and CB) over the entire UV−vis−NIR spectral range were at 226−283 nm (Figure 2B, Table 2). The peak at ∼260 nm may represent the plasmon absorption of tubular graphite.[29] The origin of this high absorbance of carbon-based NPs such as SWNTs in the NIR is expected to be from electronic transitions between the first or second van Hove singularities of the nanotubes.[30,31] By comparison, absorbance maxima for the Cu NPs (40, 60, and 80 nm) over the entire UV−vis−NIR spectral range was at 1150−1154 nm for the 60 and 80 nm Cu NPs (Figure 2C, Table 2) with the 40 nm Cu NPs displaying an additional peak at ∼800 nm (Figure 3C) suggesting additional interactions in the NIR region for smaller NPs.

Therefore, when NPs of different composition were prepared at the same concentration (50 μg/mL), the greatest spectral absorbance in the NIR range at 700 nm ($A_{700\ nm}$) was for the nanosized CB at $A_{700\ nm}$ = 0.3 relative units compared to maximum absorbance values $A_{700\ nm}$ = 0.02 for the Cu NPs. By comparison, very similar results to the CB NPs were obtained for biofunctionalized carbon nanohorns in phosphate buffered saline (PBS) with absorbance maxima at 700 nm ($A_{700\ nm}$ = 0.29) for a 150 μg/mL concentration and concentration-dependent increases of $A_{700\ nm} \approx 0.5$ at a concentration of 300 μg/mL.[2] Furthermore, surfactant stabilized highly purified SWNTs, surfactant stabilized unpurified SWNTs and oxidized MWNTs all generated greater NIR absorbance than the CB NPs with maximum absorbance values of $A_{700\ nm}$ = 0.8, 0.6, and 0.4 at 700 nm, respectively,[14] which may be due to greater concentration (100 μg/mL), better dispersion, or the inherent differences in the nanotubes.

3.2. Laser Set-up. A 500W fiber laser with a minimum power output of 30W was used as the 1064 nm continuous wave laser source. To reduce the laser power delivered to the NP solutions down to either 2.2W (0.175 W/mm^2 power density) or 4.5 W (0.358 W/mm^2 power density), a series of beam splitter were used (Figures 3 and 4). Further, to cause the entire beam to enter the 4 mm-wide cuvette that was holding the solutions during the experiments, the 8 mm beam diameter of the fiber laser was reduced to 4 mm by inserting a reversed 2× beam expander into the beam path (Figures 3 and 4). A thermocouple was placed inside the cuvette containing NP solutions with care taken to avoid the direct path of the laser beam in order to minimize any direct heating of the thermocouple by the laser (Figures 3 and 4B). A schematic of the finalized experimental setup is shown in Figure 3, and photographs of the setup are shown in Figure 4.

3.3. Visible Evidence of Heating. The different nanoparticle (NP) solutions were analyzed for temperature kinetics after laser

Table 2. Summary of Nanoparticle Physicochemical Properties

particle type	shape	1° Size (TEM)	avg. agglom. size (DLS, PDI)	charge (mV)	cell viability[a] (%)	max UV−vis−NIR absorb. @1064 nm	max Δ temp (°C)
copper oxide NPs (Cu40 nm)	irregular	78 ± 21 nm	365 nm (0.226)	0.0727	17	0.008	11
copper oxide NPs (Cu60 nm)	irregular	80 ± 31 nm	606 nm (0.301)	−1.22	18	0.007	11
copper oxide NPs (Cu80 nm)	irregular	87 ± 41 nm	537 nm (0.272)	33.4	19	0.018	11
silver (Ag) NPs	spherical	27.5 ± 9.1 nm	147 nm (0.545)	−39.5	52	0.085	25
nanosized carbon black (CB)	spherical	28.4 ± 7.6 nm	1486 nm (0.521)	−23.4	85	0.273	46
SWNTs	tubular	0.5−2 μm length, 1−2 nm diam.	200 nm (0.361)	−35.8	49	0.062	18
SWNT-COOH	tubular	0.5−2 μm length, 1−2 nm diam.	1172 nm (0.823)	−30.4	n/a	0.093	20

[a] 50 μg/mL, 24 h.

radiation at a wavelength of 1064 nm. Upon turning the laser beam on, the initial temperature was recorded, and the subsequent temperature was recorded every 30 s for 4−5 min, after which the laser was turned off. Figures 5 shows pictures of the solutions before laser exposure, after 2.2 W laser exposure, and after 4.5 W laser exposure, respectively.

In every solution, during every experiment, a certain amount of evaporation and condensation occurred, as small droplets of the solutions would form on the inside walls of the cuvette just above the surface of the solution, but no visible color change occurred. However, in the SWNT-COOH (Figure 5A−C) and CB (Figure 5D−F) solutions, bubbles formed in the solution.

3.4. NIR-Induced Nanoparticle Temperature Kinetics. Figure 6 shows the results for the change in temperature that occurred to each of the solutions over time at powers of 2.2 W (Figure 6A) and 4.5 W (Figure 6B). An empty cuvette and H2O filled cuvette served as blank and solution controls, respectively, which experienced no heating or very minimal changes in temperature upon laser irradiation. For the NP solutions, the nanosized CB particles demonstrated the greatest increase in temperature at both power settings after 4−5 min. For example, at the lower (2.2 W) power, the temperature elevation for the nanosized CB solution was ΔT_{max} = 17 °C after 4 min compared to modest temperature elevations ranging from ΔT_{max} = 6−8 °C for the SWNT, Ag, and SWNT-COOH solutions, respectively. By comparison, at the higher (4.5 W) power, the temperature elevation maximum for the nanosized CB solution was ΔT_{max} = 46 °C after 5 min, followed by ΔT_{max} = 25 °C for SWNT-COOH, ΔT_{max} = 20 °C for Ag NPs, ΔT_{max} = 18 °C for SWNTs, and ΔT_{max} = 10−12 °C for the control H_2O solution and Cu NPs.

The carboxylic acid functionalized SWNTs (SWNT-COOH) demonstrated a greater increase in temperature at both powers tested compared to the nonfunctionalized SWNTs. By comparison, the solutions of Cu NPs at all sizes (40, 60, and 80 nm) did not heat with any appreciable difference from the control vial of H2O at either laser power.

A linear rate of heating was observed for most of the solutions at the laser powers of 2.2 and 4.5 W (Figure 6C). However, the CB NPs did not have a linear rate of heating at higher temperatures because of phase changes taking effect. In this case, the rate of heating for CB was determined for temperatures below 50 °C so phase change would not affect the results.

The rates of heating were then compared with the absorption properties of the solutions as shown in Figure 7. Here, there is a linear progression where the rate of heating is proportional to the absorption properties of the particles at 1064 nm.

3.4. Theoretical Thermodynamic Modeling of Nanoparticle Heating. Modeling of the heat loss (Q_{out}) into the environment performed based upon experimental data collected after the laser was turned off (Figure 8). These data were inputted into eqs 1 and 2, whereas Q_{in} was equal to zero, in order to obtain Q_{out}. Cooling data were taken from all trials in order to model Q_{out}. It was assumed that physical and thermodynamic properties of the solutions would not be affected by the nanoparticles. Figure 8 shows a good correlation between the temperature of solution and the heat loss. This correlation corresponds to Q_{out} in order to predict the heating kinetics of the solutions (Tables 3 and 4).

The theoretical model was compared with the experimental data to determine if it is sufficient to model the heating kinetics. The difference between the experimental data and model was taken at each time point and then averaged (Tables 3 and 4). The peak temperature difference between the theoretical and experimental was also determined. For simplicity, the difference sizes of Cu NPs were not listed.

The theoretical model demonstrated good agreement with the experimental data (<20% variance) and the peak temperatures for most of the aqueous NP solutions. However, discrepancies begin to arise between the experimental data and theoretical model for the higher absorbing NPs such as CB. This can be assumed to be due to phase change, as evidenced by bubble formation/condensation, which is not taken into account in the uniform heating model of thermodynamic analysis.

4. DISCUSSION AND CONCLUSIONS

After continuous exposure to NIR (λ = 1064 nm) at powers of 2.2 and 4.5 W, various aqueous solutions of NPs (nanosized carbon black, single-walled carbon nanotubes, silver nanoparticles and copper nanoparticles) at 50 μg/mL concentrations show differential heating. The basis of this heating is due to the strong intrinsic optical absorbance of certain NPs in the NIR spectral window, which causes electrons to become excited and release excess energy in the form of heat. Therefore, these results demonstrate the utility of using NPs to convert NIR photon energy into thermal energy with high thermostability over short durations of exposure.

4.1. Relationship between Heating Kinetics, UV−vis−NIR Spectra, and Aggregation. A general trend for NP solution heating, at either laser power, can be summarized as follows: CB > SWNT-COOH > Ag NPs > SWNTs > (H_2O, Cu NPs) > empty cuvette. As expected, the control water blank had a low change in temperature (ΔT_{max} values = 4 and 11 °C at 2.2 and 4.5 W, respectively). This is in agreement with other experiments

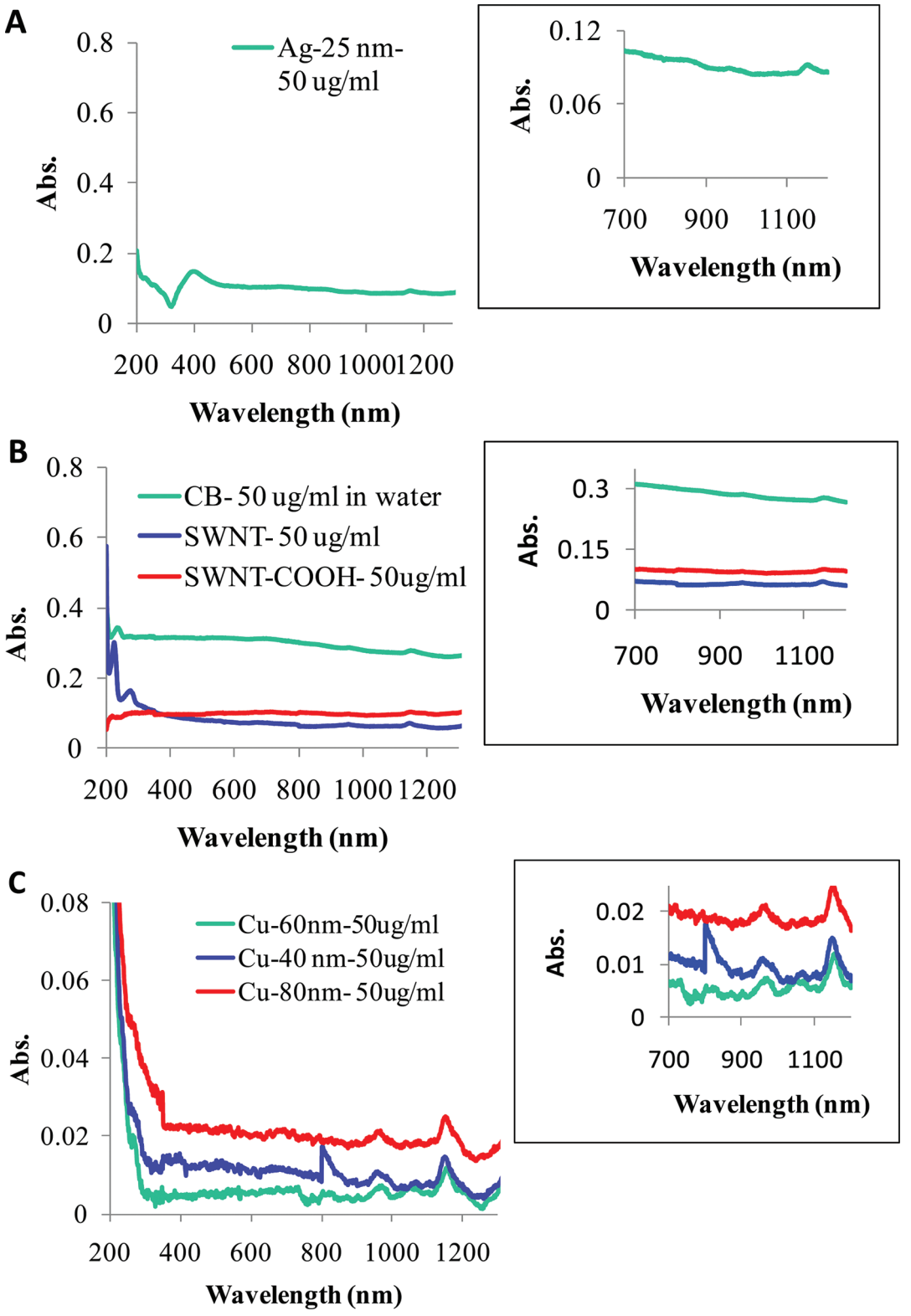

Figure 2. UV−vis−NIR spectra for NP solutions with background subtraction for water. (A) Ag NPs (B) SWNTs, SWNT-COOH, CB, and (C) Cu NPs. Insets are enlargements of the NIR region from 700 to 1100 nm. Note that the *y*-axis for absorbance is 10-fold higher for the Ag NPs and C-based NPs (CB, SWNT, SWNT-COOH) compared to the Cu NPs, which have much lower absorbance. Also note that the *y*-axis is different in each enlargement for clarity.

where continuous laser exposure (λ = 808 nm, 1.4 W/cm^2),[1] (λ = 1064 nm, 1−5 W)[2] over 2−5 min to aqueous control solutions such as phosphate buffered saline (PBS) or water led to temperature changes ranging from ∼21 to ∼30 °C.

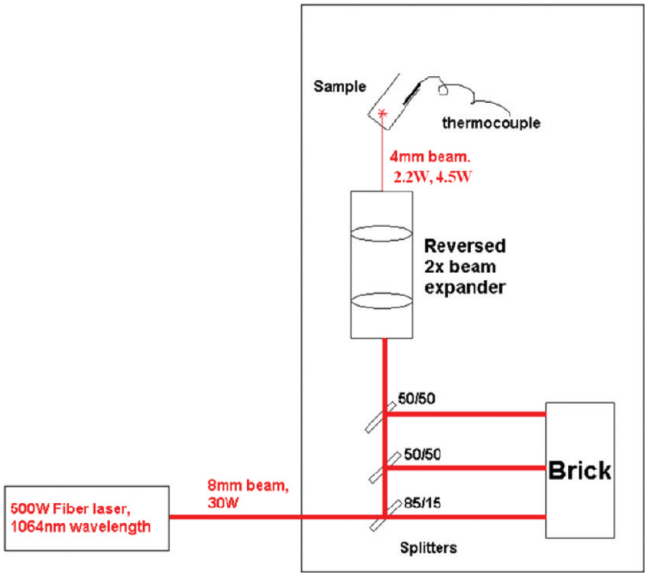

Figure 3. Schematic of the laser irradiation system. The 500 W fiber laser (1064 nm wavelength, continuous wave) was run through a series of splitters and a reverse beam expander to provide a 4 mm diameter collimated beam. A small thermocouple placed in the NP solutions was used to measure temperature.

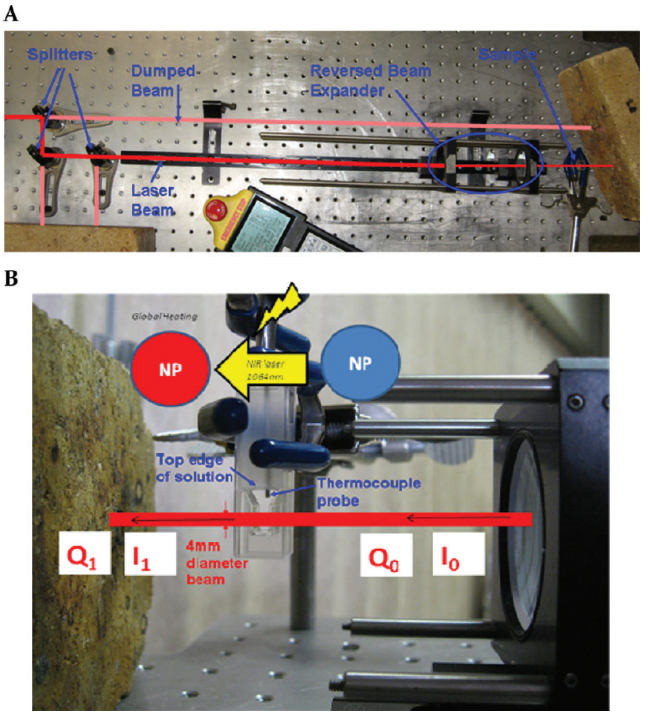

Figure 4. Digital images of experimental laser setup and parameters. Note that the red lines labeled "Laser Beam" are edited into the picture in order to represent the real laser beam path. (A) Overview of laser design. (B) Digital image of cuvette containing solution and thermocouple probe. There is no concern about the sample volume for depth-of-focus because the beam is recollimated; any liquid within the 4 mm diameter of the cuvette received the same amount of laser fluence. Notice that the thermocouple was placed at the top of the cuvette with care taken to avoid direct exposure of the thermocouple by the laser beam.

The greatest increases in temperature were for the nanosized carbon black (CB, ΔT_{max} = 46 °C, T_{max} = 67 °C) and oxidized single-walled carbon nanotubes (SWNT-COOH, ΔT_{max} = 25 °C, T_{max} = 46 °C), respectively, after the longest exposure time of 5 min and the highest power density tested of 35.8 W/cm^2. In a similar study,[5] with a 10-fold lower power density (λ = 1064 nm, 3 W/cm^2), a maximum temperature of 51 °C was reached for 100 μg/mL MWNTs after a short 30 s laser exposure. By comparison, only a very modest increase of 4 °C to a maximum temperature of 27 °C was obtained for an identical SWNT solution suggesting that different types of carbon nanotubes behave distinctly upon NIR irradiation.[5]

Concurrently, the nanosized CB and SWNT-COOH displayed the most intense absorption in the NIR region when examined with UV−vis−NIR spectroscopy. In comparison, the other NP solutions followed the same general trends for absorbance in the NIR region as the temperature changes summarized above: CB > SWNT-COOH > Ag NPs > SWNTs > Cu NPs. One exception was that the SWNT-COOH sample experienced much greater changes in heating (ΔT_{max} values = 8 and 25 °C at 2.2 and 4.5 W, respectively) compared to the Ag NPs (ΔT_{max} values = 7 and 20 °C at 2.2 and 4.5 W, respectively), although they both had almost identical absorbance at 700 nm ($A_{700\ nm}$ values = 0.1).

The greater heating for SWNT-COOH may be due to differences in the purity, size, or dispersion of the carboxylic-acid functionalized SWNT-COOH sample compared to the other NPs. However, quantitatively describing the aqueous dispersion of nanotubes is difficult and "solubility"is typically discerned through visible observations, various optical techniques and cryo-TEM. For example, Kam et al.[1] found much greater temperature elevations for well-dispersed, solubilized DNA-conjugated SWNTs (25 μg/mL) compared to nondispersed SWNTs after continuous irradiation (λ = 808 nm, 1.4 W/cm^2) resulting in a linear relationship between time and laser-induced heating from ~25 to ~70 °C in 2 min. Furthermore, Miyako et al.[2] later demonstrated that biofunctionalized CNHs displayed greater dispersion and temperature elevations up to 85 °C compared to oxidized CNHs (25 μg/mL, in PBS, λ = 1064 nm, 5 min, 5W) which were only up to 39◦C. The authors proposed that the uncondensed CNH complexes, which have a large surface area, more effectively absorbed light leading to the greater temperature elevations for the water-dispersible CNH complexes compared to insoluble CNH−COOH or CNH. Similar to these studies, we demonstrated that aggregates of carbon-based NPs with enhanced absorption in the NIR spectral window experienced the greatest heating (i.e., aggregate sizes of ~1486 and 1172 nm for CB and SWNT-COOH, respectively).

The great variation between the maximum UV−vis−NIR absorption values for the NP solutions and wavelength of laser used were found to be directly related to the temperature changes for the NP solutions. For example, the lowest temperature elevations were produced by the Cu NPs, which was related to the low absorbances around wavelengths of 1064 nm for the laser used in this study (Table 2). Therefore, even with the limitations of nonideal dispersion and inherent differences due to elemental composition, initial screening of the NP solutions with UV−vis−NIR spectroscopy for absorption in the NIR window still appears to be a rapid method for accurately predicting the resultant NP solution temperature profiles after NIR irradiation.

4.2. Role of NP Composition in Heating. Although the focus of this study was not to compare any one composition of NP,

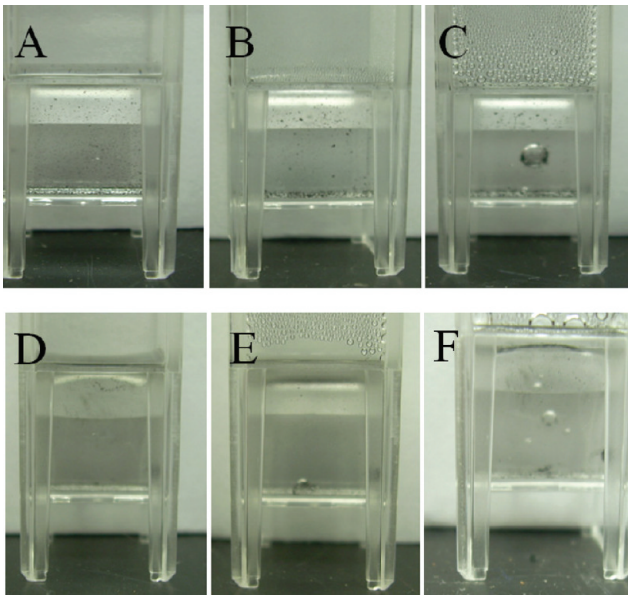

Figure 5. Digital images of representative cuvettes before and after laser exposure. (A−C) SWNT-COOH and (D−F) CB. (A, D) Before exposure, (B, E) after 2.2 W for 7 min, (C, F) after 4.5 W for 8 min. Notice the bubbles and condensate for both NP solutions after 4.5 W.

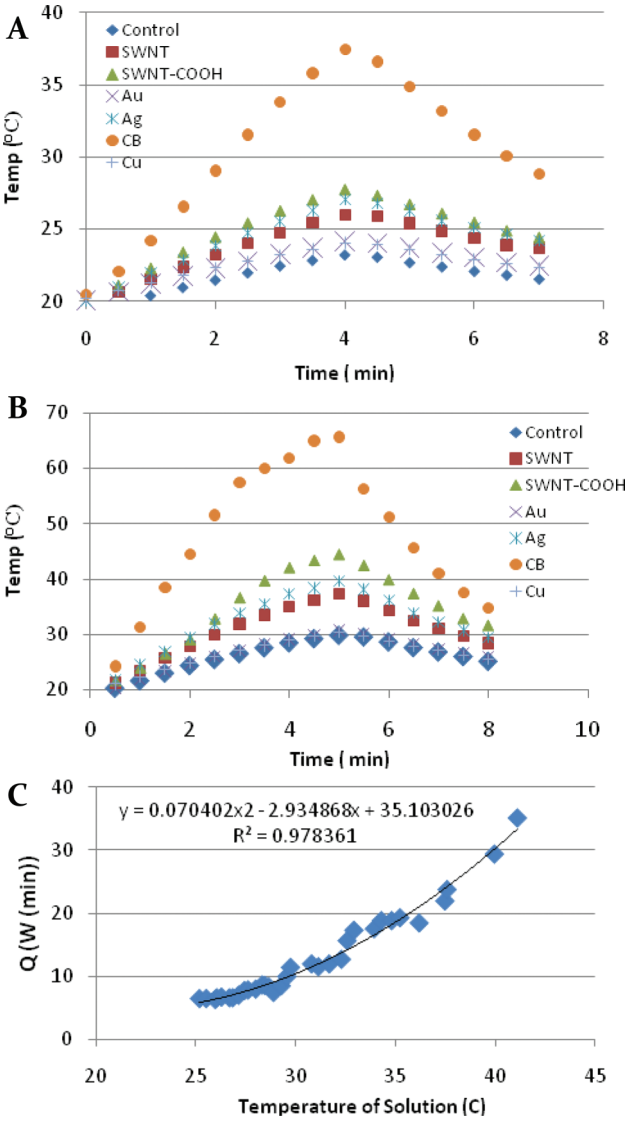

Figure 6. Experimental heating kinetics of NP solutions irradiated with (A) 2.2 W laser power measured at 30 s intervals over 7 min, (B) 4.5 W laser power measured at 30 s intervals over 8 min, and (C) experimental heat loss from the cuvette as a function of temperature of solution.

carbon-based nanomaterials are demonstrating great utility in NIR-based technologies. For this reason, we examined three different carbon-based NPs with different morphologies and surface chemistries including CB, SWNT and SWNT-COOH. We found that the small, spherical CB NPs displayed increased absorbance and temperature elevations compared to the single-walled carbon nanotubes. Other studies reported that relatively low concentrations (100 μg/mL) of surfactant stabilized (1 wt %/wt Pluronic F127 surfactant) multiwalled carbon nanotubes (MWNTs) suspended in physiologic saline were more efficient at producing a NIR-dependent increase in temperature compared to raw SWNTs (λ = 1064 nm, 3 W/cm^2, 30 s).[5] The authors attributed this phenomena to the MWNTs behaving as highly efficient dipole antennae, with broad absorption spectra compared to the specific resonance absorptions of SWNTs, making them amenable to stimulation by a range of NIR energy sources.[1,32] However, it is currently unknown why CB NPs would heat more efficiently than SWNTs because the size, shape, and other physicochemical properties of the two materials are quite different.

4.3. Role of Aggregate Size in NP Absorbance and Heating. Three different samples of Cu NPs were examined (40, 60, and 80 nm), but there were no obvious changes in the UV−vis−NIR absorbance or heating for the Cu NP solutions. One explanation for this behavior may be nonideal dispersion leading to similar sizes in solution for the 60 and 80 nm Cu NPs (~600 nm vs ~364 nm for Cu-40 nm). Because the number of NPs in the same volume of solution was is higher for the smaller NPs, the thermal effects likely depend upon both the size and the total number of NPs in suspension. Zharov et al. separated the effects of size and concentration on NIR-induced heating by selecting different diameters of gold nanospheres and nanoshells ranging from 20, 40, 60, and 100 nm compared to 130 nm by normalizing the NP concentrations to an equal 5.6 × 10^8 NPs/mL. In this case, the maximum effect was observed for the largest NPs.[3,4] However, in this study, concentration was held constant between all of the samples and the number of particles for the different sizes of Cu samples did not appear to affect the heating or absorption. Furthermore, the oxidation and irregularity in the sizes of the Cu NPs are not ideal for size-dependent studies, but rather provide new information on oxidation-dependent effects where the smaller Cu NPs contain more surface oxides.

4.4. Visible Solution Changes: Bubble Formation. Visual examination of the nanosized CB and SWNT-COOH solutions demonstrated evidence of bubble formation and condensation on the upper portions of the quartz cuvettes after reaching maximum bulk temperatures of 48 and 68 °C, respectively. A similar study by Miyako et al. described bubble formation prior to boiling (85 °C) after 5−10 min of NIR laser exposure (λ = 1064 nm, 5W) for highly concentrated 200 μg/mL CNHs in PBS.[2] They concluded that the effective transient local temperature around the NPs must have also been at least ≥85 °C. Because these temperatures are lower than the boiling temperature of water (100 °C), it is likely that a mechanism involving

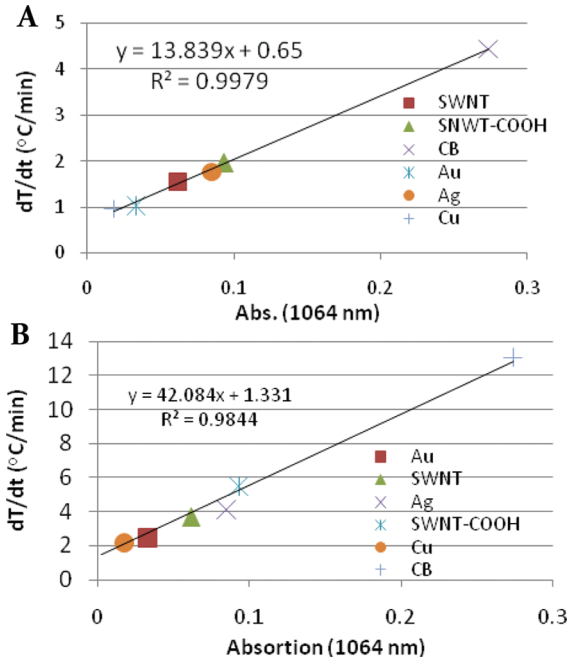

Figure 7. Comparison of the absorption of the solutions at 1064 nm with the rate of heating: (A) 2.2 W laser and (B) 4.5 W laser.

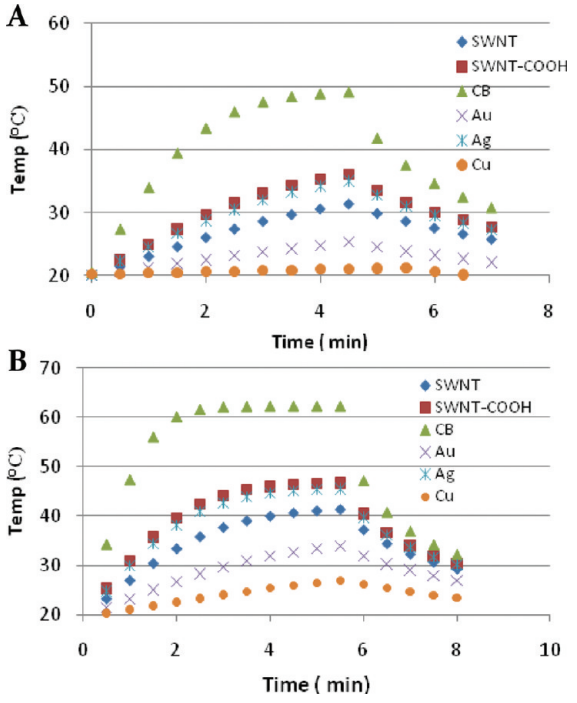

Figure 8. Theoretical heating kinetics of NP solutions irradiated with (A) 2.2 W laser power measured at 30 s intervals over 7 min and (B) 4.5 W laser power measured at 30 s intervals over 8 min.

localized heating around the NPs is responsible for the gas evolution. For example, superheating can occur near the nanoparticle surface upon exposure to NIR leading to temperatures of several hundred degrees Celsius prior to boiling of the bulk solution dependent upon the nanoparticle size.[8] These superheated particles will cause bubbles to form rapidly around the particle. Bubble formation was seen for the SWNT-COOH samples (Figure 5) which indicates that the particles are becoming superheated. These values have practical implications in the use of NPs to very discrete locations in individual cells and disease tissues (i.e., cancer cells, subcellular organelles) where targeted delivery can effectively heat and destroy selected cells while avoiding healthy cells.

Table 3. Comparison of Theoretical to Experimental Data for 2.2 W Laser

	avg % diff (test)	peak temp diff
SWNT	12.32	5.32
SWNT-COOH	18.91	8.26
CB	26.91	11.63
Au	1.66	1.11
Ag	18.66	7.94
Cu	8.43	2.77

Table 4. Comparison of Theoretical to Experimental Data for 4.5 W Laser

	avg % diff (test)	peak temp diff
SWNT	11.25	4.00
SWNT-COOH	13.19	2.13
CB	16.04	3.28
Au	7.29	3.06
Ag	15.59	7.33
Cu	9.26	3.53

In addition to the bulk heating temperature measured, the size of the NP aggregates plays a role in bubble formation. For example, small NPs tend to display low thermal and bubble-formation effects because of low heating efficiency resulting from lower NP absorption.[33] This may partially explain the intense NIR absorption, heating and bubble production by large bundles of SWNTs (micrometers in length). In agreement with this notion, DNA-conjugated SWNTs formed gas bubbles and began to boil after >2 min of continuous laser irradiation (λ = 808 nm, 1.4 W/cm^2).[1]

In this study, the thermodynamic modeling based upon uniform heating supports the notion that phase transformation, in the form of solution bubbling, is a viable mechanism for alterations in the experimental thermal profiles.

4.5. Role of Surface Chemistry/Charge on Dispersion and Heating. When comparing the effect of surface functional groups, the carboxylic-acid functionalized single-walled carbon nanotube (SWNT-COOH) samples experienced a greater temperature elevation, as well as evidence of possible gas generation, compared to their nonoxidized SWNT counterparts. One possible explanation for this behavior is the better solution stability (dispersion) and subsequent stronger NIR absorption profile of the SWNT-COOH compared to the SWNTs. However, it is very difficult to systematically describe the dispersion of nanotubes solutions with techniques such as dynamic light scattering, which is based on the scattering of light from spherical particles. In the case of nanotubes, the values for aggregate size or overall solution dispersion result from both diameter and length values leading to sometimes irreproducible and inaccurate values. For example, in this study, we obtained average size values of 200

and 1172 nm for the SWNT and SWNT-COOH samples, respectively.

Furthermore, higher zeta potentials, or increasingly negative or positive charges, on the surface of the NPs may provide some degree of interparticle or interaggregate separation, which may influence the heating kinetics. However, in this study, there was no direct link between zeta potential and NP heating; all of the NPs had negative surface charge except for the Cu NPs. Along these lines, surface functionalities that dissociate may influence the bulk solution properties such as pH, ion content and specific heat. However, in this study, there were no intention surface modifications. Although the acid purified SWNTs contained carboxylic acid surface functionalities (SWNT-COOH), the surface groups were residual artifacts from the purification process. Of course, other postsynthesis NP modifications should be considered for their effects upon NP heating in addition to purposeful surface functionalization, for example, with biomolecules for targeting and delivery.

4.6. Limitations and Future Research. Although the temperature of the NP solutions was examined throughout the duration of the laser exposure every 30 s for up to 8 min, we did not vary the concentrations of NPs in the solutions, which were all prepared at a constant mass-basis concentration of 50 μg/mL. However, it is expected that increasing the concentration of some of the NPs may lead to further elevation of temperature with an eventual threshold saturation plateau. Support for this notion was found in studies with carbon nanohorns (CNHs) where laser exposure (λ = 1064 nm, 5W, 5 min) to solutions of 25 μg/mL CNHs in PBS resulted in heating up to ~55 °C compared to more highly concentrated 200 μg/mL samples, which reached temperatures >85 °C and boiled after 5−10 min.[2] When comparing different carbon-based NPs, one study found that a 2000 μg/mL (2 mg/mL) concentration of SWNTs was required to generate a temperature elevation to >50 °C (increase of ~27 °C), which was the equivalent heating of a 20-fold lower concentration (100 μg/mL) of MWNTs.[5] Although SWNTs were comparable with MWNTs in inducing a temperature increase at the upper limit of concentrations tested (1000−2000 μg/mL), It was hypothesized that the bundling and scattering effects of nanotubes are minimized at much lower concentrations (100 μg/mL), which can result in MWNTs displaying greater temperature increases compared to SWNTs.[5] However, in the above studies, it was not ruled out that other factors (such as actual number of NPs per volume) contributed to the differential effects since there are a substantially greater number of smaller NPs in the same volume compared to the number of larger particles.

Varying the duration of NIR laser (λ = 1064 nm, 3 W/cm^2) exposure from 15 to 60 s resulted in a temperature threshold between 50 and 55 °C was reached within 30 s for a 100 μg/mL suspension of MWNTs.[5] It was also shown that a much greater temperature elevation occurred for well-dispersed DNA-conjugated SWNTs (25 μg/mL) after continuous irradiation (808 nm, 1.4 W/cm^2), which resulted in a linear relationship between time and laser-induced heating from ~25 to ~70 °C in 2 min.[1]

By comparison, the carbon-based nanomaterials in this study (CB, SWNT-COOH, SWNT) prepared at 50 μg/mL heated to 67, 46, and 39 °C (respectively) after the maximum exposure duration of 5 min with continuous 1064 nm laser irradiation. These values are highly consistent with the temperature trends presented above for carbon-based nanomaterials at concentrations ranging from 25 to 200 μg/mL and for similar laser power and time conditions (λ = 808−1064 nm, 5 W, 5−10 min). Therefore, varying the NP core composition and surface functionality, NP concentration, NP number, laser exposure duration and other experimental factors will be critical for understanding optimal heating profiles and developing NP-based therapeutics.

5. CONCLUSIONS

This study reveals the differential heating kinetics of NPs excited with NIR with implications in the development of novel NIR-NP based systems. The laser conditions used in this study (λ = 1064 nm, 2.2−4.5 W, up to 5 min, volume ~1 mL) demonstrated effective heating. From a practical perspective, tailoring the NP composition and other physicochemical properties (i.e., size, surface chemistry, etc.) should lend to better control of interactions occurring at the interface between NPs and NIR laser light for applications in evolving fields such as nanomedicine. Therefore, future research should focus on the high importance of understanding the detailed molecular mechanisms at work, which can be translated to real-world scenarios and conditions.

AUTHOR INFORMATION

Corresponding Author
*E-mail: saber.hussain@wpafb.af.mil.

ACKNOWLEDGMENT

A.M.S. received funding from the National Research Council (NRC) Fellowship program funded by the Joint Science and Technology Office for Chemical and Biological Defense (JSTO−CBD), a program administered by the Defense Threat Reduction Agency (DTRA). B.M.S. received funding from ORISE at AFRL/RHPB. Clearance #88ABW-2011-3894.

NOMENCLATURE:

m = mass of water in cuvette (grams)
C_v = heat capacity at const. volume (J/(g k))
Q_{in} = energy flow into system (J/s)
Q_{out} = energy flow out of system (J/s)
T_2 = current temperature of solution (K)
T_1 = initial temp. of solution (K)
T = transmittance
I_1 = light passing through solution
I_o = initial light going into the solution
TR = light transmittance
a = measured absorption of solution at (1064 nm)
P = power of laser beam (w/mm^2)
A = cross-sectional area of laser beam (mm^2)

REFERENCES

(1) Kam, N. W. S.; O'Connell, M.; Wisdom, J. A.; Dai, H. *Proc. Natl. Acad. Sci. U.S.A.* **2005**, *102*, 11600–11605.
(2) Miyako, E.; Nagata, H.; Hirano, K.; Makita, Y.; Nakayama, K.-I.; Hirotsu, T. *Nanotechnology* **2007**, *18*, 103–110.
(3) Zharov, V. P.; Galitovskaya, E. N.; Johnson, C.; Kelly, T. *Laser Surg. Med.* **2005**, *37*, 219–226.
(4) Zharov, V. P.; Kim, J.-W.; Curiel, D. T.; Everts, M. *Nanomedicine* **2005**, *1*, 326–345.
(5) Burke, A.; Ding, X.; Singh, R.; Kraft, R. A.; Levi-Polyachenko, N.; Rylander, M. N.; Szot, C.; Buchanan, C.; Whitney, J.; Fisher, J.; et al. *Proc. Natl. Acad. Sci. U.S.A.* **2009**, *106*, 12897–12902.

(6) Burda, C.; Chen, X.; Narayanan, R.; El-Sayed, M. A. *Chem. Rev.* **2005**, *105*, 1025–1102.
(7) Bendix, P. M.; Reihani, S. N. S.; Oddershede, L. B. *ACS Nano* **2010**, *4*, 2256–2262.
(8) Kyrsting, A.; Bendix, P. M.; Stamou, D. G.; Oddershede, L. B. *Nano Lett. 11* **2011**, 888–892.
(9) Urban, A. S.; Fedoruk, M.; Horton, M. R.; Rädler, J. O.; Stefani, F. D.; Feldmann, J. *Nano Lett.* **2009**, *9*, 2903–2908.
(10) Letfullin, R. R.; George, T. F.; Duree, G. C.; Bollinger, B. M. *Adv. Opt. Tech.* **2008**, 718–726.
(11) Pustovalov, V. K. *Chem. Phys.* **2005**, *308*, 103–108.
(12) Schrand, A. M.; Dai, L.; Schlager, J. J.; Hussain, S. M.; Osawa, E. *Diamond Relat. Mater.* **2007**, *16*, 2118–2123.
(13) Schrand, A. M.; Braydich-Stolle, L. K.; Schlager, J. J.; Dai, L.; Hussain, S. M. *Nanotechnology* **2008**, *19*, 104–117.
(14) Joshi, A.; Punyani, S.; Bale, S. S.; Yang, H.; Borca-Tasçiuc, T.; Kane, R. S. *Nat. Nanotechnol.* **2008**, *3*, 41–45.
(15) Torti, S. V.; Byrne, F.; Whelan, O.; Levi, N.; Ucer, B.; Schmid, M.; Torti, F. M.; Akman, S.; Liu, J.; Ajayan, P. M.; et al. *Int. J. Nanomed.* **2007**, *2*, 707–714.
(16) Chakravarty, P.; Marches, R.; Zimmerman, N. S.; Swafford, A. D.-E.; Bajaj, P.; Musselman, I. H.; Pantano, P.; Draper, R. K.; Vitetta, E. S. *Proc. Natl. Acad. Sci. U.S.A.* **2008**, *105*, 8697–8702.
(17) Rey, D. A.; Strickland, A. D.; Kirui, D.; Niamsiri, N.; Batt, C. A. *ACS Appl. Mater. Interfaces* **2010**, *2*, 1804–1810.
(18) Tollan, T. M.; Marcilla, R.; Pomposo, J. A.; Rodriguez, J.; Aizpurua, J.; Molina, J.; Mecerreyes, D. *ACS Appl. Mater. Interfaces* **2009**, *1*, 348–352.
(19) Gao, Z.; Zhi, C.; Bando, Y.; Golberg, D.; Serizawa, T. *ACS Appl. Mater. Interfaces* **2011**, *3*, 627–632.
(20) Hirsch, L. R.; Stafford, R. J.; Bankson, J. A.; Sershen, S. R.; Rivera, B.; Price, R. E.; Hazle, J. D.; West, J. L. *Proc. Nat. Acad. Sci. U.S.A* **2003**, *100*, 13549–13554.
(21) Loo, C.; Lowery, A.; Halas, N.; West, J.; Drezek, R. *Nano Lett.* **2005**, *5*, 709–711.
(22) El-Sayed, I. H.; Huang, X.; El-Sayed, M. *Cancer Lett.* **2006**, *239*, 129–135.
(23) Huang, X.; El-Sayed, I. H.; Qian, W.; El-Sayed, M. A. *J. Am. Chem. Soc.* **2006**, *128*, 2115–2120.
(24) Gobin, A. M.; O'Neal, D. P.; Watkins, D. M.; Halas, N. J.; Drezek, R. A.; West, J. L. *Laser Surg. Med.* **2005**, *37*, 123–129.
(25) Anderson, R. R.; Parrish, J. A. *Science* **1983**, *220*, 524–527.
(26) Soller, E. C.; Hoffman, G. T.; McNally-Heintzelman, K. M. *Biomed. Sci. Instrum.* **2002**, *38*, 339–344.
(27) Murdock, R. C.; Braydich-Stolle, L.; Schrand, A. M.; Schlager, J. J.; Hussain, S. M. *Toxicol. Sci.* **2007**, *101*, 239–253.
(28) Skebo, J. E.; Grabinski, C. M.; Schrand, A. M.; Schlager, J. J.; Hussain, S. M. *Int. J. Toxicol.* **2007**, *26*, 135–141.
(29) Isobe, H.; Tanaka, T.; Maeda, R.; Noiri, E.; Solin, N.; Yudasaka, M.; Iijima, S.; Nakamura, E. *Angew. Chem., Int. Ed.* **2006**, *45*, 6676–6680.
(30) O'Connell, M. J.; Bachilo, S. M.; Huffman, C. B.; Moore, V. C.; Strano, M. S.; Haroz, E. H.; Rialon, K. L.; Boul, P. J.; Noon, W. H.; Kittrell, C.; et al. *Science* **2002**, *297*, 593–596.
(31) Bachilo, S. M.; Strano, M. S.; Kittrell, C.; Hauge, R. H.; Smalley, R. E.; Weisman, R. B. *Science* **2002**, *298*, 2361–2366.
(32) Hirsch, L. R.; Gobin, A. M.; Lowery, A. R.; Tam, F.; Drezek, R. A.; Halas, N. J.; West, J. L. *Ann. Biomed. Eng.* **2006**, *34*, 15–22.
(33) Huttmann, G.; Birngruber, R. *IEEE J. Sel. Top. Quantum Electron.* **1999**, *5*, 954–962.